Thermoelectric properties of ZnO ceramics densified through spark plasma sintering

P.M. Radingoana[a], S. Guillemet-Fritsch[a,*], J. Noudem[b], P.A. Olubambi[c], G. Chevallier[a], C. Estournès[a]

[a] *CIRIMAT, Université de Toulouse, CNRS, Université Toulouse 3 - Paul Sabatier, 118 Route de Narbonne, 31062, Toulouse cedex 9, France*
[b] *Normandie Univ, Ensicaen, Unicaen, Cnrs, CRISMAT, 14000, Caen, France*
[c] *University of Johannesburg, School of Mining, Metallurgy and Chemical Engineering, Johannesburg, South Africa*

ABSTRACT

Thermoelectric properties of pure ZnO ceramics were investigated in this study. ZnO powders were sintered using spark plasma sintering by varying temperature (600–900 °C) and atmosphere (air and vacuum), thereafter, the ceramics were annealed in air at 600 °C. Relative densities > 98% were determined for all the samples with grain sizes of the same order of magnitude, hence, thermal conductivity of ~45 W/mK was determined at room temperature. As-sintered ceramics prepared from synthetic powder (CSP) had higher carrier concentration than ceramics prepared from commercial powder (CCP) by 2.3×10^{17} cm^{-3}. Thus, resistivity and Seebeck Coefficient of 0.08 Ω cm and 475 μV/K were determined, respectively, at room temperature for CSP sintered at 900 °C. There was no significant change on the performance of the ZnO ceramics when the sintering atmosphere and temperature were altered. Annealing did not improve the thermoelectric properties of ZnO ceramics. Maximum ZT of 8×10^{-3} was obtained for CSP sintered at 900 °C.

1. Introduction

The rising demand of energy (especially in developing countries such as South Africa, China and India) is estimated to increase further to meet the future's global economy [1 5]. However, the consequences of using fossil fuels make the supply of energy very difficult as it runs a risk of causing global warming/climate change. Nowadays, government and private companies both national and international collaborate to meet the future energy demands by improving research and develop ment in energy sectors, exploring different energy sources and im proving and conserving energy efficiency in current operations. Ther moelectric power generation has interested most researchers for the past decades; it involves direct conversion of heat to electricity [6 10]. This method can be used without any pollution and be applied in confined spaces. It is mainly being used to recover wasted heat from motor vehicles, industries etc … The performance of the thermoelectric materials (*both n and p type*) is being measured by the figure of merit, ZT, which is defined as $ZT = \frac{S^2}{\rho k}T$ whereby S is the Seebeck Coefficient, ρ is resistivity and k is thermal conductivity [7].

Recently, many research studies have been focused on developing new materials and exploring new preparation techniques to get higher ZT, above 2 [8,11]. Materials such as Si Ge alloys, rare earth chalco genides and transition metal disilides have been extensively in vestigated for high temperature thermoelectric applications [12 17]. However, these materials are costly which limits large scale application. They also require surface protection against oxidation. Metal oxides were found to be suitable materials for long term application at high temperatures [18 21]. The *n type*, zinc oxide (ZnO) has shown appro priate characteristics for thermoelectricity such as high Seebeck Coef ficient and could easily be formulated (chemically) in view to improve electrical properties [21]. Most of all it is environmentally friendly and contains earth abundant elements.

Extensive research on ZnO ceramics has been performed on the doping and the dual doping with group 3 elements and transition me tals [21 28]. However, there is limited literature that focuses on the thermoelectric properties of pure ZnO ceramics. The performance of ZnO relies mostly on the concentration of oxygen vacancies [29]. Therefore, it is vital to have better understanding of the electrical properties of intrinsic ZnO. Other means which have been conducted to improve thermoelectric properties of ZnO ceramics is applying nanos tructuring [30,31]. This method reduces thermal conductivity through phonon scattering at the grain boundaries. The advancements in sin tering techniques from conventional pressing to spark plasma sintering

have added huge value on the control of grain growth. However, some reports have indicated that even though reducing the grain size could assist in lowering the thermal conductivity, it can also lower the electrical conductivity due to the scattering of electrons [31].

In this work, efforts were made on the preparation method for ZnO powder and compare its characteristics with those of commercial powder. Microstructural studies of the sintered ceramics at various sintering conditions were investigated in detail. The thermoelectric properties of the ZnO ceramics were discussed for both as sintered and annealed in air to have better understanding on the effect of oxygen vacancies.

2. Materials and methods

2.1. Materials

ZnO nanopowders synthesized using co precipitation method followed by calcination was used in this study. The powders labelled as C500, C600 and C700 have grain sizes of 78 ± 19, 177 ± 61 and 289 ± 154 nm, respectively. The surface area of the powders is 14.5, 5.9 and 3.3 m²/g *for* C500, C600 and C700, *respectively*. The synthesized ZnO powder was compared with those of commercially available zinc oxide (Com ZnO) of high purity (99.99%) which had a grain size and surface area of 193 ± 111 nm and 5.8 m²/g.

2.2. Densification of ZnO by spark plasma sintering (SPS)

The commercial and synthesized ZnO powders were densified using SPS already descrbed in the previously published paper [32] using 8 and 20 mm inner diameter tungsten carbide and graphite dies. The molds were lined with 0.2 mm thick graphite foil (PERMA FOIL®Toyo Tanso). Sintering parameters (such as temperature (600 900 °C) and atmosphere (air and vacuum)) were investigated with the aim to have fully dense pellets with minimal grain growth. Samples sintered in vacuum were current isolated to avoid the influences of electric field on the ZnO grains; which can affect the reactivity and diffusion during sintering [33,34].

The uniaxial pressure up to 250 MPa was applied at room temperature for the samples sintered at 600 and 700 °C, using tungsten carbide tool for 2 min. On the other hand, the conventional graphite mould has been used under vacuum. The pressure of 100 MPa was applied for samples sintering at 900 °C on last the 2 min of heating stage to improve mobility of grains. The temperature increase was at a ramp up speed of 100 °C/min, though for samples sintered at 900 °C the ramp up speed was reduced by 50% on the last 2 min of heating stage to avoid temperature overshoot. The isothermal time was kept for 6 min.

The temperature was cooled at a rate of 100 °C/min simultaneously with pressure release.

2.3. Characterization of ZnO ceramics

The microstructure analysis of the ZnO ceramics were done using Scanning Electron Microscopy (MEB JEOL JSM65 10LV) while an X ray diffractometer (XRD Bruker D4) was used to analyze the phase struc ture. A combination of Differential Thermal Analysis (DTA) and ther mogravimetric analysis (DAT GTA) (Setaram, TAG16) was used to study the thermal behaviour of the sintered ceramics at a heating rate of 3 °C/min up to 1000 °C.

2.4. Electrical measurements

The electrical measurements were conducted at Laboratoire de Cristallographie et Sciences des Matériaux (CRISMAT). Seebeck Coefficient and resistivity of the dense ceramics were simultaneously measured using ZEM 3 (Ulvac Riko). The dense ceramics were cut into 9x3x3 mm bars and coated with gold to ensure electrical ohmic contact. Graphite foil was inserted on both sides of heaters to have a good electrical and thermal contact with the sample. The thermal conductivity was determined by measuring separately thermal diffusivity (α), ceramic density (d) and heat capacity (Cp) (Eq. (1)). The samples were cut to dimensions of $6 \times 6 \times 1$ mm.

$$k = \alpha(T)Cp(T)d(T) \tag{1}$$

The band gap was determined through the photovoltaic route using Bentham PVE 300 PV, 20 mm diameter ceramics with a thickness of 0.5 mm. The hall effect measurements were done using physical property measurement system (Model 7100 AC transport controller, Quantum system), by measuring 3×3 mm square samples.

3. Results and discussions

3.1. Spark plasma sintering of pure ZnO ceramics

This section discusses the spark plasma sintering of commercial and synthetic ZnO powder in order to compare the influence of the starting powder characteristics on densification and microstructural evolution of ZnO ceramics. The effect of sintering temperature and atmosphere are investigated, the summary of the relative density and grain size evolution of the ceramics are presented in Table 1. The ZnO ceramics prepared from synthetic and commercial powder are abbreviated as CSP and CCP, respectively.
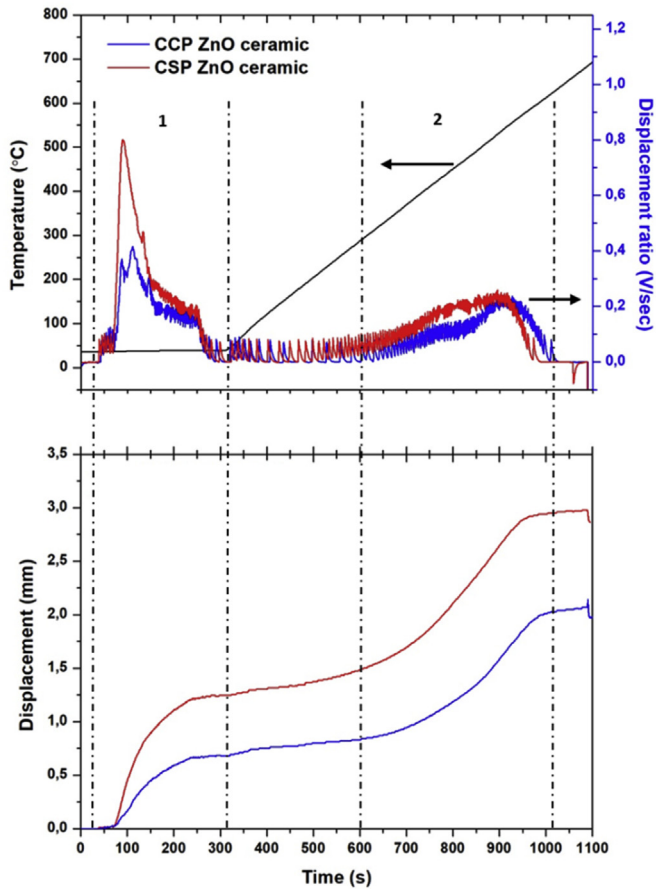
Table 1
Relative density and grain size of ceramics prepared from com-ZnO and synthetic ZnO powder for different sintering conditions **[Symbols: CCP is ceramics prepared from commercial ZnO powder, CSP is ceramics prepared from synthetic ZnO powder, SC is sintering cycle and RT is room temperature]**.

Die diameter	Atmosphere	Sintering cycle	Insulation	Temperature	Pressure & when applied	Relative density	Grain size (Image J)
mm	–	–	–	°C	MPa	%	μm
Powder calcined at 500 °C (C500)							
8	Air	SCI	Without	600	250,RT	100	2,2 ± 0.6
8	Air	SCI	Without	700	250,RT	99.4 ± 0.2	6 ± 2
Powder calcined at 600 °C (C600)							
8	Air	SCI	Without	600	250,RT	99.3 ± 0.1	2,4 ± 0.6
8	Air	SCI	Without	700	250,RT	99.5 ± 0.2	5,4 ± 1.3
20	Air	SCI	Without	700	250,RT	100	5 ± 2
20	Vacuum	SC2	With	900	100, Last 2 min of heating stage	98.9 ± 0.4	4 ± 2
Powder calcined at 700 °C (C700)							
8	Air	SCI	Normal	600	250,RT	99.3 ± 0.2	3 ± 1
8	Air	SCI	Normal	700	250,RT	100	4,2 ± 1,6
Commercial ZnO (Com-ZnO)							
8	Air	SCI	Without	700	250,RT	97,8 ± 1,2	5,3 ± 2,3
20	Air	SCI	Without	700	250,RT	99,1 ± 0,5	5,4 ± 2,1
20	Vacuum	SC2	With	900	100, Last 2 min of heating stage	98,7 ± 0,4	3,6 ± 1,3

Fig. 1. Displacement ratio and displacement during heating of pure commercial and synthetic ZnO powder in air (700 °C).

3.1.1. Sintering behaviour of commercial and synthetic pure ZnO in air and vacuum

3.1.1.1. Sintering in air atmosphere. The sintering behaviour of the commercial and synthetic ZnO powders was studied in air up to a temperature of 700 °C (the temperature limit of the tungsten carbide tools) while keeping a constant axial pressure of 250 MPa, without current isolation. Synthetic powder calcined at 600 °C was used as it has almost the same average grain size as the commercial powder: 177 ± 61 nm (synthetic powder) and 193 ± 111 nm (commercial powder). The punch displacement and displacement ratio, representing respectively the shrinkage and shrinkage speed of the powder, are given in Fig. 1 as a function of sintering time. The displacement ratio of both samples showed two peaks: sharp peaks at 100 300s (room temperature) and broad peaks at 600 1000s (300 600 °C). The first peak could be attributed to the rearrangement of grains by rolling due to applied pressure at room temperature [32,35,36]. The second peak could be due to the densification of the ceramics at high temperature, with grains diffusing with neighbouring grains. The influence of sintering temperature on ceramics prepared through commercial powder (CCP) has been published [32].

During the heating stage, the displacement of both samples gradu ally increases with temperature and tend to reach a constant state after 900s. The ceramics prepared from synthetic ZnO powder (CSP) reach higher displacement of about 3 mm as compared to the commercial powder (CCP) (2 mm). This could be due to the smaller particles size distribution and homogenous morphology, leading to better mobility of grains [37 39]. It was also observed that CSP finished sintering earlier than the CCP with a difference of ~40 °C. This indicates the importance of working with nano sized grains that can be sintered at lower tem perature. The sintering mechanism of pure ZnO in air could be con trolled by the lattice and grain boundary diffusion of interstitial Zn ions (Zn_i) [40 44]. ZnO being a non stoichiometric material, it is sensitive to sintering atmosphere, which could affect the densification of the ZnO ceramics. This discussion is detailed in section 3.1.1.2.

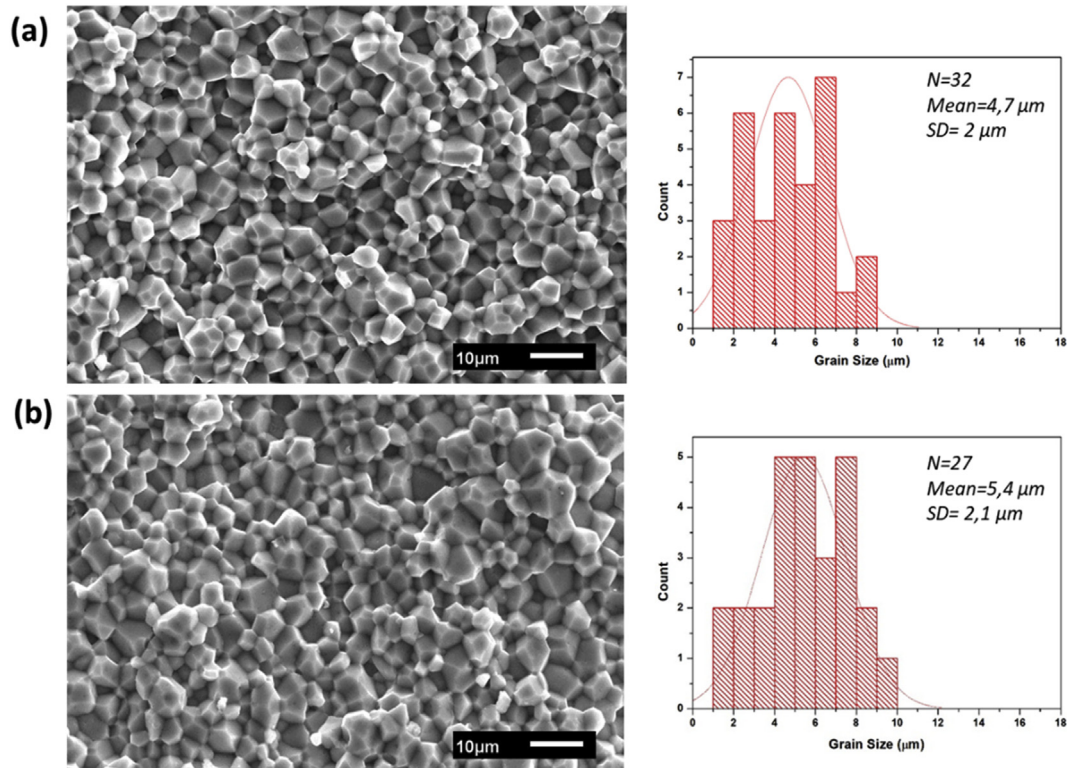The CSP and CCP ceramics were sintered at a dwell time of 6 min.

Fig. 2. SEM micrograph of fractured surfaces and grain size distribution (Image J) (a) CSP ceramic (b) CCP ceramic (700°C-250 MPa).
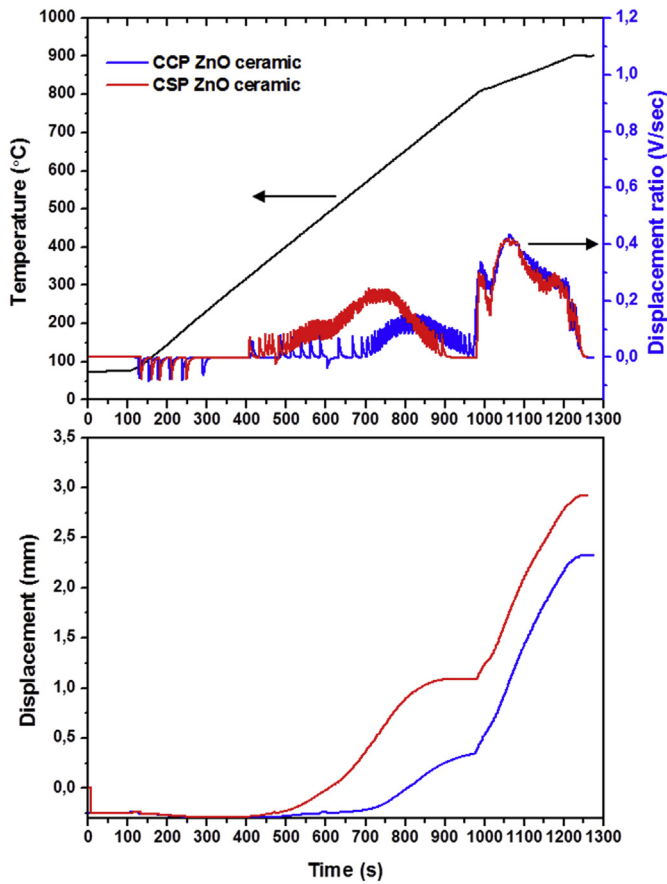
Fig. 3. Displacement ratio and displacement during heating of pure commercial and synthetic ZnO powder in air (900 °C).

The relative densities are given in Table 1. No significance difference was observed for both powders sintering at 700 °C, the relative density of CSP and CCP was 100% and 99%, respectively. The SEM micrographs of CSP and CCP ceramics are given in Fig. 2. The same grain size dis tribution for both ceramics is evidenced. The grain size increased from 177 nm to 4.7 μm for CSP and from 193 nm to 5.4 μm for CCP, in dicating samples present same growth rate. The grain size distribution of both samples indicated to be similar. XRD patterns indicated no phase change after sintering.

3.1.1.2. Sintering in vacuum atmosphere. Commercial and synthetic ZnO powders were further sintered in vacuum to evaluate the sintering behaviour of the ZnO ceramics up to a temperature of 900 °C, applying axial pressure of 100 MPa on the last 2 min of heating stage, with current isolation. Insulation was used in this section to avoid the influence of electric field on the ZnO grains because sintering ZnO at high temperature creates more oxygen vacancies which could affect the consistency of current flow. The punch displacement and displacement ratio, representing respectively the shrinkage and shrinkage speed of the powder, are given in Fig. 3 as a function of sintering time. The displacement ratio of both samples showed two broad peaks at 400 900s (200 600 °C) and 1000 1250s (800 900 °C). The first peak could be caused by the softening of the grains during the heating stage, as a result the grains easily rearrange [35 37]. It was observed that CSP ceramics shrinks at 400 °C, 300s earlier than CCP ceramics. This could have occurred because of differences in particle size distribution and morphology in the starting powders. Han et al. [45] reported about the sintering of Al doped ZnO ceramics prepared from nanoparticles, rods and platelets powders. Similar relative densities of 90% were reported, though it was observed that the rods and platelets ceramics have preferential orientation on miller impedance, < 001 >, direction while for the nanoparticles it was prohibited. Whereas, Zhang et al. [46] reported on Al doped ZnO ceramics with hybrid micro/nano structure powders. In this case, low relative density of 80% was achieved with non preferential grain growth. These findings could support the
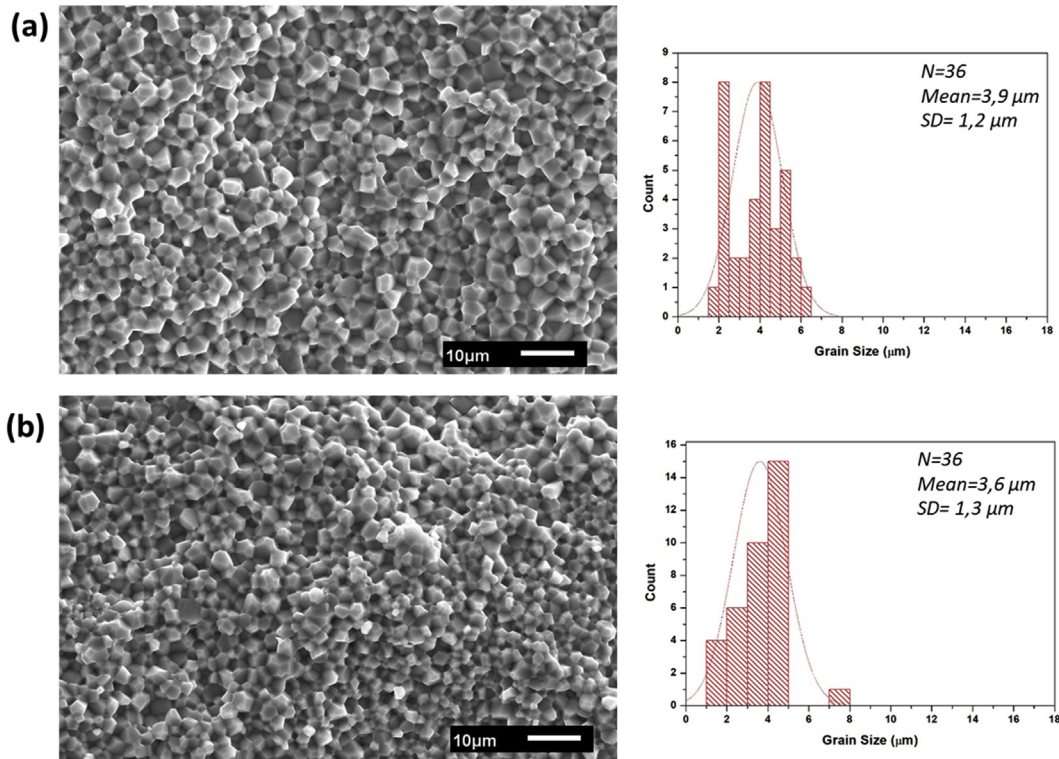

Fig. 4. SEM micrograph of fractured surfaces and grain size distribution (Image J) (a) CSP ceramics (b) CCP ceramic (900 °C   100 MPa-SC2).

observed unique sintering behavior of CCP and CSP ceramics due to the differences in powder quality.

The second peak (Fig .3) could be caused by applied pressure. It was observed that during the heating stage, the displacement of both sam ples gradually increases with temperature and tend to reach a constant state after 1200s. The CSP and CCP ceramics reached displacement of about 3 and 2.5 mm, respectively. As previously stated, the difference could be due to smaller particle size distribution and morphology of CSP powder which leads to higher mobility of grains.

The powders were sintered under dwell period of 6 min and the relative densities are presented in Table 1. The relative density of CSP slightly decreased to 98.9% when sintering in vacuum at 900°C, this could have resulted from the presence of pores in the ceramic [37]. Similar relative density was achieved for CCP. The microstructure given in Fig. 4 revealed that there is no significant change in the grain size as well between CSP and CCP, an average mean grain size of 3.9 μm and 3.6 μm were determined, respectively. Comparing the two sintering temperatures (700°C and 900°C), CSP grain size remained at a mean of 4 μm when sintering at 700°C and 900°C. While a slight decrease in the grain size was observed in CCP, from 5.4 μm (700°C) to 3.6 μm (900°C). Smaller grain sizes were obtained at 900 °C because of axial pressure was applied on the last minutes of heating stage; this delayed the dif fusion of grains at the grain boundaries.

3.1.2. Effect of sintering temperature on synthetic ZnO powder

Synthetic powders were prepared through the co precipitation process followed by calcination. Then, the samples were sintered at 600 °C and 700 °C for comparison using 8 mm die. The ceramics were labelled as C500, C600 and C700 for the starting powders calcined at 500 °C, 600 °C and 700 °C, respectively. The relative densities given in Table 1 showed that fully dense ceramics above 99% are obtained for the ceramics prepared from synthetic powder. It was noted that the behaviour of densification differs for each powder; C500 reach 100% densification at 600 °C while increasing the temperature to 700 °C leads to a decrease of 0.6%. Whereas, increasing the temperature from 600 °C to 700 °C in C700 ceramics resulted an increase in the relative density from 99.3 100%. The difference could have been caused by the differ ence in powder surface area; C500 had higher surface area of reaction as compared to C700. Similar results were reported by Aimable et al. [47] on comparative study of sintering synthesized and commercial powder. The relative density of C600 ceramics did not change much when the temperature was increased.

The XRD analyses of the ceramics presented in Fig. 5 indicated no change in the phase structure. It is a hexagonal wurzite structure of

Fig. 5. XRD patterns of ZnO ceramics from synthesized powder sintered at 600 °C.

ZnO; similar characteristic signature was observed for all the para meters. The SEM micrographs of the fractured surfaces of the ceramics sintered at 600 °C and 700 °C are reported in Fig. 6. It was observed that, at both temperatures, sintering leads to homogenous morphology and an increase in the grain size for C500, C600 and C700 ceramics. At a temperature of 600 °C, grain size of 2.2, 2.4 and 3 μm were de termined for C500, C600 and C700 ceramics, respectively. Further in crease in the temperature to 700 °C caused a decrease in the grains from 6, to 5.4 and 4.2 μm for C500, C600 and C700 ceramics, respectively. The sample C500 showed bigger grains as compared to C600 and C700, probably because of the high surface area of reaction which results in surrounding grain boundaries easily diffuse with each other as ex plained earlier [28,47].

3.1.3. Influence of annealing treatment on the microstructure of ZnO ceramics

The ZnO ceramics sintered at 700 °C prepared from commercial powder (Com ZnO) were used to study the influence of annealing on the microstructural properties. The as sintered ZnO ceramics were an nealed in air to oxidise the ceramic to have stable electrical measure ments. Annealing in oxygen environment fills the available oxygen vacancies and breaks the donor complex, this improves the resistivity measurements [29]. The thermogravimetric analysis of the as sintered ZnO ceramic shown in Fig. 7 indicated a logarithmic increase in mass from 0 to about 0.24% when the temperature was increased. This in dicates that the oxygen from the atmosphere reacts with interstitials Zn^{2+} to form stable compound ZnO, see Eq (2) [48,49]. The inserted photographs showed that the ceramic changes colour from greyish to white when it is annealed in air. Based on the TGA results, the ceramics were annealed during 24 h at 600 °C in air to stabilize the stoichiometry in the ceramics. The SEM microstructure of the annealed ceramic after 24 h is presented in Fig. 8; it was observed that grain size difference between the as sintered and annealed is insignificant. This will be beneficial in improving the thermal conductivity as small grain size could be quite useful.

$$Zn^{2+} + \frac{1}{2}O_2(g) \leftrightarrow ZnO\ (s) \tag{2}$$

3.2. Thermoelectric properties of pure ZnO ceramics

3.2.1. Influence of microstructure and ZnO defects on thermoelectric properties

3.2.1.1. Resistivity of ZnO ceramics. The resistivity results of various ZnO ceramics as a function of temperature are presented in Fig. 9; all samples showed an increase in the resistivity with an increase in temperature indicating a typical metallic behaviour. Gautam et al. [23] observed similar electrical behaviour on pure ZnO, however, the causes of such behaviour was not reported. Similar behaviour was observed for Ni doped ZnO ceramics at temperatures between 250 450 °C, the behaviour was due to thermally induced disconnection of low ohmic chains of ZnO grains by highly resistive NiO phase [50]. In this report the ceramic is pure ZnO, therefore the only plausible explanation is that the metallic behaviour could have been caused by the presence of ZnO defects formed during sintering and/or grain boundary resistance [51].

The effect of sintering temperature on CCP ceramics sintered in a vacuum becomes evident in the resistivity behaviour. At RT both the *700°C Vacuum CCP and 900°C Vacuum CCP* samples have the same re sistivity of ~0.12 Ω cm, shown in Fig. 9. However, when the sample temperature is raised to 500 °C the resistivity's begin to deviate with that of *700°C Vacuum CCP* sample showing a more rapid increase when compared to *900°C Vacuum CCP*. This behaviour may be attributed to higher concentration of oxygen vacancies in *900°C Vacuum CCP* than in the *700°C Vacuum CCP* resulting in a slow increase in the resistivity in the former. This idea is further supported by the lower carrier mobility for the *900°C Vacuum CCP* sample when compared to that of *700°C*
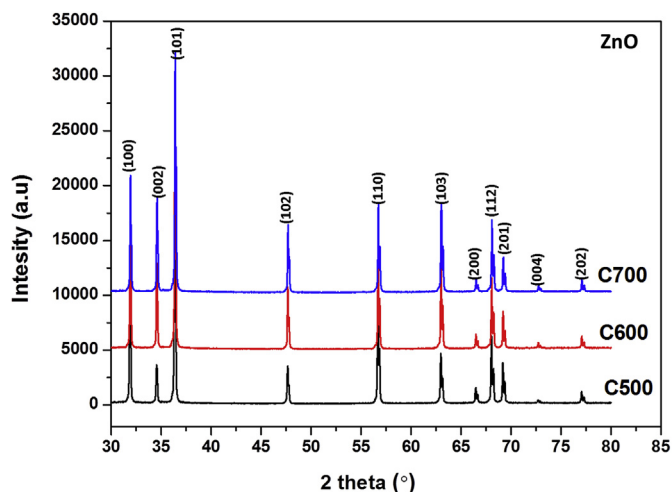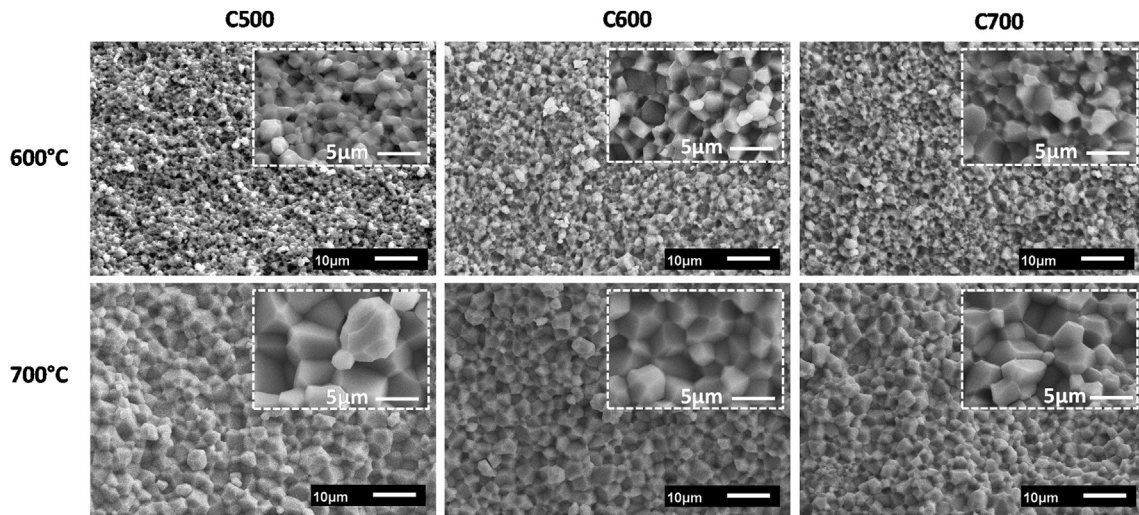
Fig. 6. SEM micrograph of fractured surfaces of ZnO ceramics prepared from synthesized powder (P = 250 MPa).
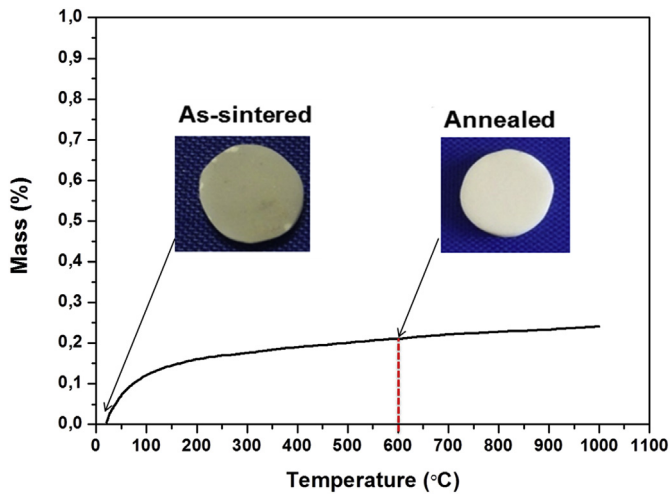

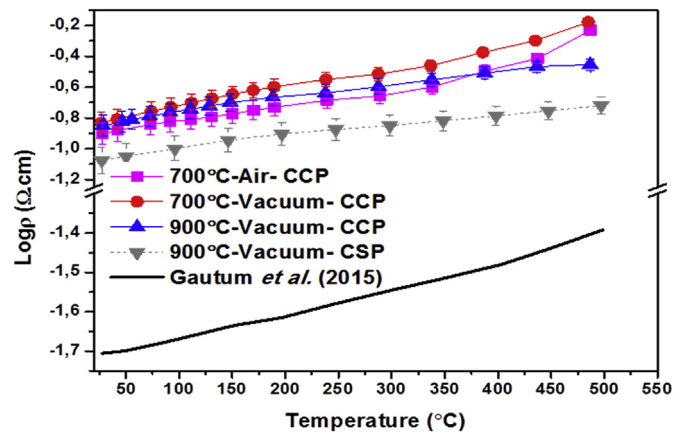Fig. 7. Thermogravimetric (TGA) analysis of as-sintered CCP ceramic.

Fig. 9. Resistivity vs temperature of as-sintered pure ZnO ceramics.

Vacuum CCP sample, see Table 2. From the additional electrical parameters of the ceramics given in Table 2 and it is shown that there is a difference of 0.7 x 10^{17} cm^{-3} in carrier concentrations between *700°C Vacuum CCP* and *900°C Vacuum CCP,* which could be another further explanation for the slow increase in the resistivity for *900°C Vacuum CCP.*

Table 2
Electrical parameters measured at room temperature of as-sintered ZnO ceramics.

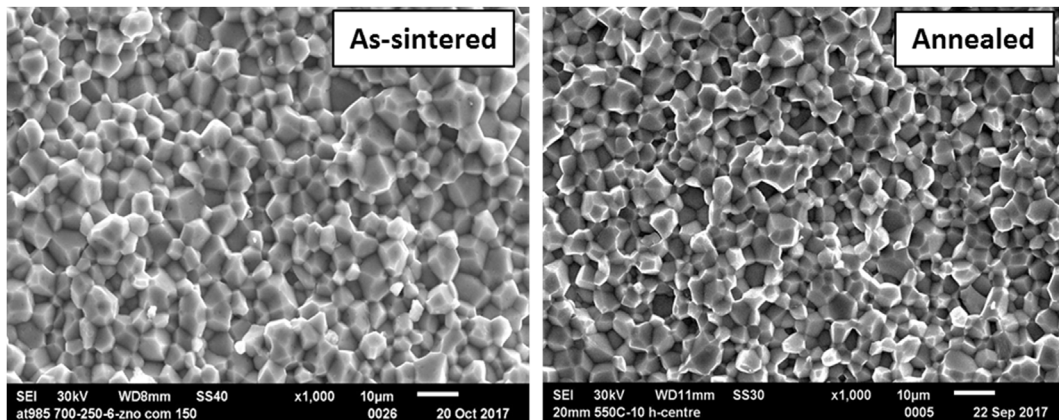| Sample	n (cm^{-3})	μ (cm/V.s)	Bandgap (eV)
700°C-Air-CCP	4,3x10^{17}	116	3.1
700°C-Vacuum-CCP	4,8x10^{17}	90	3.2
900°C-Vacuum-CCP	5,5x10^{17}	83	3.1
900°C-Vacuum-CSP	7,8x10^{17}	62	2.9

Fig. 8. SEM micrographs of as-sintered and annealed CCP ceramic.

From the resistivity measurements, Fig. 9, the influence of the sintering atmosphere on the electrical behaviour on CCP ceramics is not very significant. It is noted however that between 150 °C and 400 °C it is observed that *700°C Air CCP* undergoes some chemical changes due to oxidation resulting in a lower resistivity as compared to the *700°C Vacuum CCP*. This process ceases above 450 °C probably due to saturation and the resistivity of the two samples become comparable.

The influence of the synthesis process on the electrical behaviour was further evaluated by comparing the resistivity behaviour of two samples; commercial CCP and synthetic CSP, both sintered at 900 °C in vacuum. It was observed that *900°C Vacuum CSP* was the most conducting of all the samples i.e. lower resistivity compared to *900°C Vacuum CCP* and all other samples. Although the sample still showed metallic behaviour with increase in temperature like other samples it was however always lower than all samples in resistivity. This could be because of the high carrier concentration of $7.8 \times 10^{17}\ cm^{-3}$ and even though it has low mobility caused, probably by oxygen vacancies and defects. The reported resistivity values for ZnO are higher than the ones reported in literature; this could be because of the difference in ceramic preparation conditions [23,26,28,52]. The bandgaps of all the samples are in the same range and would not have significant influence on the differences observed in the resistivity data in Fig. 9.

3.2.1.2. Seebeck Coefficient of ZnO ceramics.

The variation of the Seebeck Coefficient (or thermopower) as a function of temperature is given in Fig. 10; the negative sign indicated *n type* conductivity. High absolute Seebeck Coefficient (|S|) values of between 550 600 µV/K were obtained for CCP samples at room temperature. Whilst for the CSP samples a lower value of $|S| 475 =$ µV/K was obtained at room temperature. Gautum et al. [23] reported even lower |S| value of 280 µV/K at room temperature. The differences in these experimental values are most likely as a result of differences in carrier concentrations in the different samples. The Seebeck coefficient is related to the carrier concentration in semiconductors as given by Mott's formula in Eq. (3) [21]. It is therefore evident that different material preparation techniques have the ability to engineer materials with unique and diverse properties. In this light different sintering technique plays a huge role on the electrical properties of ceramics, as was observed in difference in values for both Seebeck Coefficient.

From Fig. 10; it was observed that when the temperature is increased from room temperature to 500 °C there is a transition in |S| that occurs at ~325 °C for *700°C Air CCP* and *700°C Vacuum CCP* ceramics.
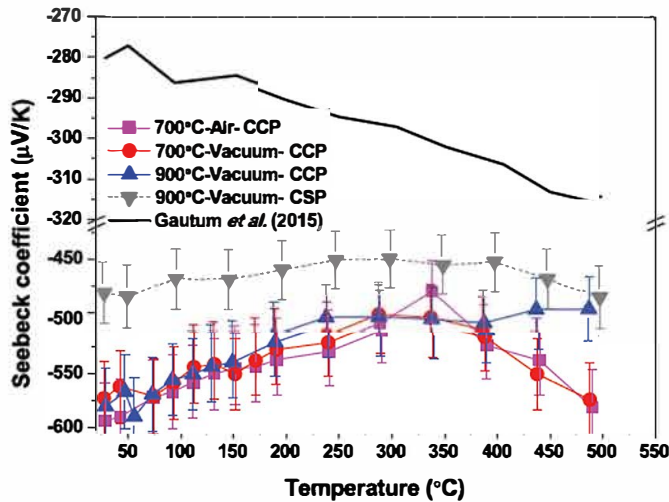
The |S| Increased from ~ 575 µV/K at room temperature to 500 µV/K at 325 °C, thereafter decreased again to 575 µV/K at 500 °C this due to the increase in more electrons (i.e. Charge carriers) being promoted above the Fermi level into the conduction band because of increase in temperature and hence more electrons moving from the hot junction to the cold junction. Above 325 °C this promotion reaches a saturation point and further increase in temperature results in electron scattering instead due to increased lattice vibrations and hence a decrease in |S| back to −575 µV/K again. The increased scattering was further supported by the increase in resistivity at high temperatures which was explained earlier.

For the *900°C Vacuum CCP* samples |S| increased up to 250 °C and thereafter remained constant with an increase in temperature suggesting that after carrier saturation there is no significant scattering to lattice vibrations, any issue which will be explored when thermal conductivity is discussed.

The 900 °C Vacuum CSP samples did not show significant changes in |S| with temperature. This is somewhat surprising and this requires further experimental work not possible at the present moment. Therefore, further studies need to be done to have better understanding on the thermoelectric properties of intrinsic ZnO ceramics especially those which are oxygen deficiency.

3.2.1.3. Thermal conductivity of ZnO ceramics.

The temperature dependence of thermal conductivity is presented in Fig. 11; it is evident that the thermal conductivity of all samples decreased with an increase in temperature due to phonon phonon scattering due to increased lattice vibrations [31]. At room temperature, the initial thermal conductivity for all samples was ~45 W/m.K and these decreases exponentially to ~12 W/m.K at 500 °C. The results are similar to the work reported by Gautam et al. [23]. However, these values are too high for improved thermoelectric applications and the reason might be due to the relatively large grain sizes of the samples. Which are namely 5.3, 5.4, 3.6, 5.4, and 3.9 µm corresponding to samples 700 °C Air CCP, 700 °C Vacuun CCP, 900 °C Vacuum CCP, 700 °C Air CSP and 900 °C Air CSP, respectively. As a result, nanostructuring is being considered as an option to reduce the thermal conductivity.

3.2.1.4. Figure of merit and power factor of ZnO ceramics.

The key thermoelectric performance behaviour of the ceramics as a function of temperature is shown in Fig. 12 in terms of power factor (Fig. 12 (a)) and figure of merit (Fig. 12 (b)). The power factor measures the electrical performance of the ceramics by comparing the Seebeck

Fig. 10. Seebeck Coefficient vs temperature of as-sintered pure ZnO ceramics.

$$S_{bulk} = \frac{8m^*\pi^2 k_b^2}{2eh^2}T\left(\frac{\pi}{2n}\right)^{\frac{2}{3}}$$
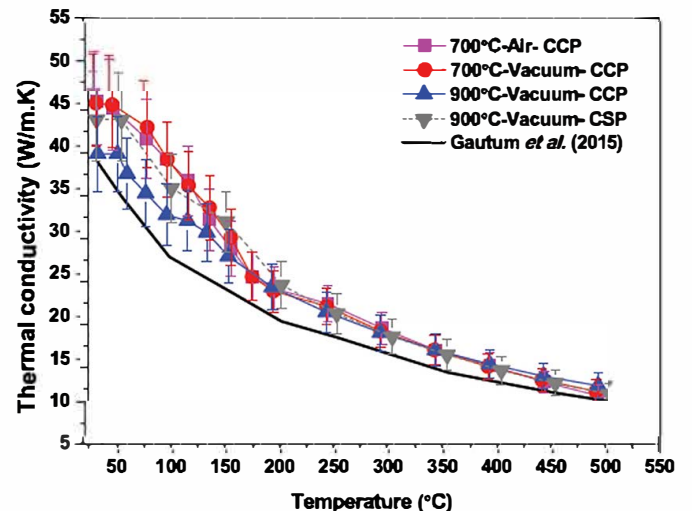
(3)

Fig. 11. Thermal conductivity vs Temperature of as-sintered pure ZnO ceramics.
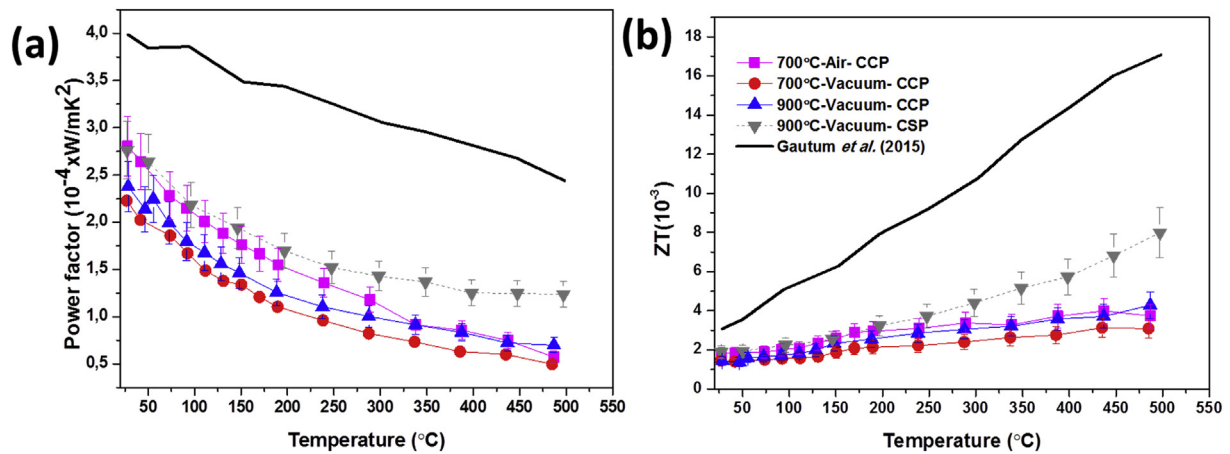
Fig. 12. Performance of as-sintered ZnO ceramics with temperature: power factor (a) ZT (b).

Coefficient and resistivity of the ceramics. From Fig. 12 (a) it is observed that 700 °C Air CCP and 900 °C Vacuum CSP ceramics gave the highest power factor of about 2.7×10^{-4} W/m^{2}K at room temperature due to the lower electrical resistivity resulting from higher carrier concentration and higher mobility. The overall decrease in the power factor with temperature could be related to the increase in the resistivity due to phonon scattering and possibly additional oxidation of the ceramics.

The figure of merit (ZT) in Fig. 12 (b) shows a general increase in ZT with an increase in temperature for all the samples. This evolution can be related to the decrease in the thermal conductivity when the temperature is increased and/or alternatively due to an increase in the Seebeck Coefficient particularly at higher temperatures. A maximum ZT of 8×10^{-3} at 500 °C was achieved for 900 °C Vacuum CSP ceramic this is not very far from that reported by Gautam et al. [23] a ZT of 17×10^{-3} at the same temperature. Further improvements the thermo electric properties requires an increase in the carrier concentration of the ZnO ceramics maybe through doping with donor elements such as Al, Ga, In etc … which is in progress.

3.2.2. Effect of annealing on thermoelectric properties

Prior to attempts on doping, some work was done to try and understand the effect of annealing on the thermoelectric properties of the ZnO ceramics. CSP ZnO ceramic sintered at 900 °C in Vacuum was annealed in air for 24 h at 600 °C. The thermoelectric properties of as sintered and annealed ceramics are indicated in Fig. 13. The annealed sample expectedly became more resistive, by four orders of magnitude at 50 °C (Fig. 13(a)). This is probably because of the decrease in the carrier concentration from 7.8×10^{17} to 5.5×10^{13} cm^{-3} as a result of ZnO oxidation when it thermally heated in air. The annealed sample indicated a semiconducting behaviour with an increase in temperature. The difference in the conduction mechanism in the samples can be attributed to differences on ZnO defects concentrations. A transition at 250 °C was observed which may have been due to the non equilibrium state of the sample. Zakutayev et al. [53] reported a transition for annealed Ga doped ZnO thin films at 500 °C. After 350 °C, the resistivity is close to that reported by Liang [26] and Sondergaard el al. [27].

The evolution of Seebeck Coefficient with temperature is given in Fig. 13 (b); the |S| increased from 500V/K to ~ 800 V/K at room temperature when annealed because of the decrease in the carrier concentration. The absolute value of the Seebeck Coefficient decreased with an increase in temperature, similarly to that of as sintered ceramics. Liang [26] reported almost constant the |S| with temperature whilst Sondergaard et al. [27] observed an increase with temperature as expected by the Mott's equation. The increase in |S| in this study has been explained earlier in section.

The thermal conductivity of the ceramics given in Fig. 13 (c)

indicated that the annealing conditions used in this study do not bring any significant difference on thermal conductivity. Thermal con ductivity of 43 W/mK at 75 °C was determined for both as sintered and annealed ZnO ceramics, which is within previously reported values of 33 48 W/mK at 75 °C [26,27].

The figure of merit vs temperature data is given in Fig. 13 (d) it reveals that annealing does not improve the performance of the ZnO ceramics probably because of reduced electrical conductivity. Max imum ZT of $\sim 2 \times 10^{-3}$ was obtained at 500 °C for annealed ZnO ceramics. The performance of both the as sintered and annealed is in the range of other reported ZT values in the literature.

4. Conclusions

The influence of sintering atmosphere and temperature on the densification and microstructure evolution of ZnO ceramics prepared from commercial and synthesized powder were successfully in vestigated. Ceramics prepared from synthetic powder could be fully densified above 99% at temperature as low as 600 °C. At temperatures around 700 °C the ZnO ceramics indicated to be sensitive to the pow der's specific surface area, ceramic's grain sizes of 6 ± 2 μm and 4.2 ± 1.6 μm were obtained for surface areas of 14 m^2/g (C500) and 3.3 m^2/g (C700), respectively. This study has illustrated that SPS can sinter to high densities irrespective of starting powder. However, to maintain a nanostructured ceramic it is important to look into low temperature sintering and/or modification of starting powder.

Annealing at 600 °C did not show any significant change on the microstructure of ZnO ceramics but changed the oxygen stoichiometry. And this had an effect on the electrical conduction mechanism as an nealed samples became semiconducting while the as sintered ceramics showed metallic behaviour.

A somewhat unique behaviour was observed on Seebeck Coefficient variation with temperature and attempts to explain this unique beha viour was given which however might need further work to confirm this behaviour.

The thermal conductivity of ZnO ceramics was found to be still too high for more efficient thermoelectric applications. And as such there is need to look into reducing the thermal conductivity by doping with donor elements such as Al, Ga, In etc as shall be shown the subsequent chapters. Annealing did not improve thermoelectric properties of the ZnO ceramics because it reduced the electrical conductivity sig nificantly.

In conclusion from this work it became apparent that sample pre paration technique is important in determining the electrical con ductivity and thermoelectric properties of materials. Ceramics prepared from synthetic powder showed higher carrier concentration than the commercial bought ceramics. As a result, as sintered ceramics prepared
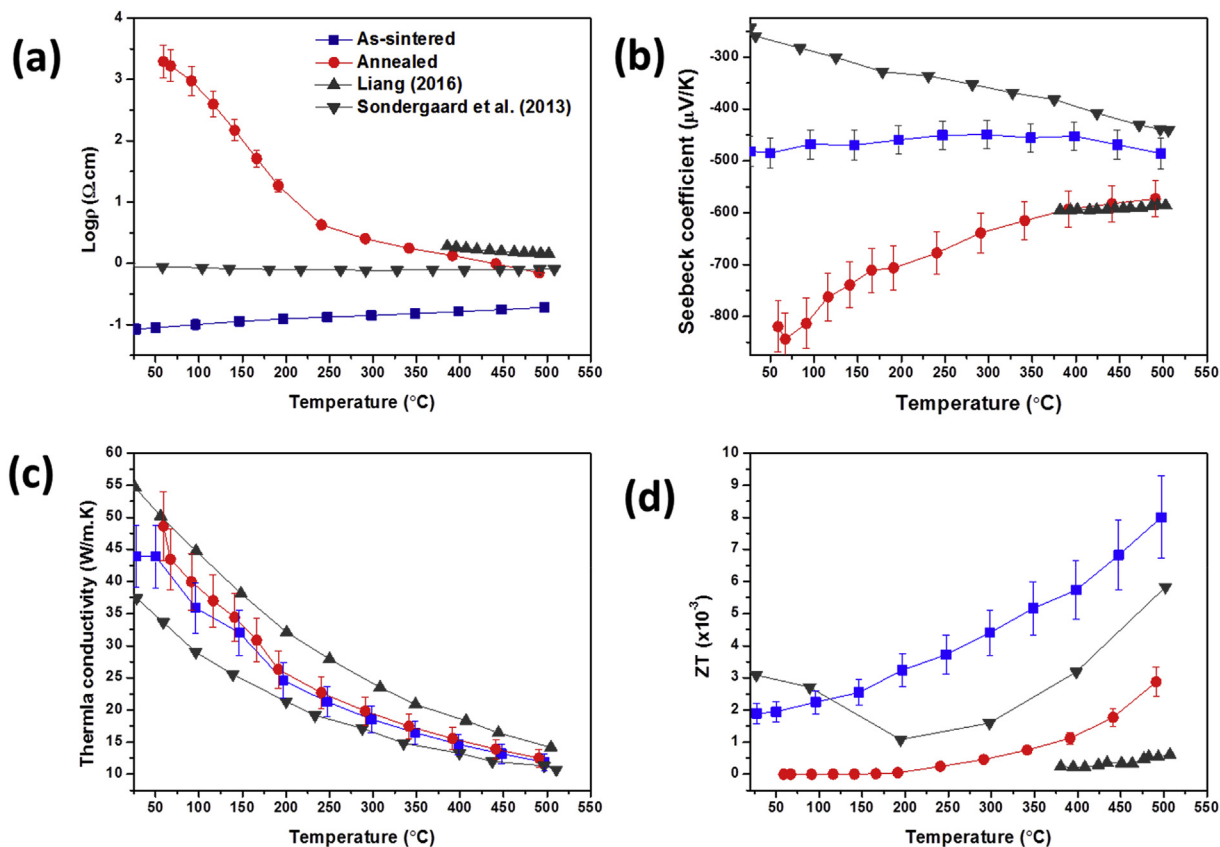
Fig. 13. Thermoelectric properties of annealed 900°C-Vacuum-CSP ceramic: (a) resistivity (b) Seebeck Coefficient (c) thermal conductivity (d) ZT.

from synthetic powder gave the best and highest performance with a ZT of 8×10^{-3} which is far much better than that from commercial samples.

Declaration of competing interest

References

[1] J. McCarthy, A socioecological fix to capitalist crisis and climate change? The possibilities and limits of renewable energy, Environ. Plan. (2015) 2485–2502, https://doi.org/10.1177/0308518X15602491.

[2] S. Muller-Kraenner, Energy Security, Routledge, 2015.

[3] O. Nematollahi, H. Hoghooghi, M. Rasti, A. Sedaghat, Energy demands and renewable energy resources in the Middle East, Renew. Sustain. Energy Rev. (2016) 1172–1181, https://doi.org/10.1016/j.rser.2015.10.058.

[4] A.P. Panel, Power People Planet: Seizing Africa's Energy and Climate Opportunities: Africa Progress Report 2015, (2015) https://app-cdn.acwupload.co.uk/wpcontent/uploads/2015/06/APP REPORT 2015 FINAL low1.pdf.

[5] S. Singer, J.-P. Denruyter, D. Yener, The Energy Report: 100% Renewable Energy by 2050. Towards 100% Renewable Energy, Springer, 2017, pp. 379–383 https://assets.panda.org/downloads/101223 energy report final print 2.pdf.

[6] J. He, T.M. Tritt, Advances in thermoelectric materials research: looking back and moving forward, Science 357 (6358) (2017) eaak9997 https://org/10.1126/science.aak9997.

[7] X. Zhang, L.-D. Zhao, Thermoelectric materials: energy conversion between heat and electricity, Journal of Materiomics (2015) 92–105, https://doi.org/10.1016/j.jmat.2015.01.001.

[8] X. Zheng, C. Liu, Y. Yan, Q. Wang, A review of thermoelectrics research–Recent developments and potentials for sustainable and renewable energy applications, Renew. Sustain. Energy Rev. (2014) 486–503, https://doi.org/10.1016/j.rser.2013.12.053.

[9] G.S. Nolas, J. Sharp, J. Goldsmid, Thermoelectrics: Basic Principles and New Materials Developments, Springer Science & Business Media, 2013.

[10] E. Maciá-Barber, Thermoelectric Materials: Advances and Applications, Pan Stanford, 2015.

[11] M. Zebarjadi, K. Esfarjani, M. Dresselhaus, Z. Ren, G. Chen, Perspectives on thermoelectrics: from fundamentals to device applications, Energy Environ. Sci. (2012) 5147–5162, https://doi.org/10.1039/c1ee02497c.

[12] R. Funahashi, S. Urata, T. Sano, M. Kitawaki, Thermoelectric properties of Ca3Co4O9 single crystals/powder composite, J. Jpn. Soc. Powder Powder Metall. (2003) 485–489, https://doi.org/10.2497/jjspm.50.485.

[13] Y. Lan, D. Wang, Z. Ren, Silicon–germanium alloys, Advanced Thermoelectrics: Materials, Contacts, Devices, and Systems (2017) 353.

[14] A. Olvera, N. Moroz, P. Sahoo, P. Ren, T. Bailey, A. Page, et al., Partial indium solubility induces chemical stability and colossal thermoelectric figure of merit in Cu 2 Se, Energy Environ. Sci. (2017) 1668–1676, https://doi.org/10.1039/c7ee01193h.

[15] D. Wu, L.-D. Zhao, X. Tong, W. Li, L. Wu, Q. Tan, et al., Superior thermoelectric performance in PbTe–PbS pseudo-binary: extremely low thermal conductivity and modulated carrier concentration, Energy Environ. Sci. (2015) 2056–2068, https://doi.org/10.1039/c5ee01147g.

[16] L.-D. Zhao, D. Berardan, Y. Lin, J.-F. Li, C.-W. Nan, et al., BiCuSeO oxyselenides: new promising thermoelectric materials, Energy Environ. Sci. (2014) 2900–2924, https://doi.org/10.1039/C4EE00997E.

[17] L.-D. Zhao, S.-H. Lo, Y. Zhang, H. Sun, G. Tan, C. Uher, et al., Ultralow thermal conductivity and high thermoelectric figure of merit in SnSe crystals, Nature (2014) 373 https://www.nature.com/articles/nature13184.pdf.

[18] Y. Feng, X. Jiang, E. Ghafari, B. Kucukgok, C. Zhang, I. Ferguson, et al., Metal oxides for thermoelectric power generation and beyond, Advanced Composites and Hybrid Materials (2018) 1–13, https://doi.org/10.1007/s42114-017-0011-4.

[19] C. Gayner, K.K. Kar, Recent advances in thermoelectric materials, Prog. Mater. Sci. (2016) 330–382, https://doi.org/10.1016/j.pmatsci.2016.07.002.

[20] G. Kieslich, G. Cerretti, I. Veremchuk, R.P. Hermann, M. Panthöfer, J. Grin, et al., A chemists view: metal oxides with adaptive structures for thermoelectric applications, Phys. Status Solidi (a) (2016) 808–823, https://doi.org/10.1002/pssa.201532702.

[21] S. Walia, S. Balendhran, H. Nili, S. Zhuiykov, G. Rosengarten, Q.H. Wang, et al.,

Transition metal oxides–Thermoelectric properties, Prog. Mater. Sci. (2013) 1443–1489, https://doi.org/10.1016/j.pmatsci.2013.06.003.

[22] H. Colder, E. Guilmeau, C. Harnois, S. Marinel, R. Retoux, E. Savary, Preparation of Ni-doped ZnO ceramics for thermoelectric applications, J. Eur. Ceram. Soc. (2011) 2957–2963, https://doi.org/10.1016/j.jeurceramsoc.2011.07.006.

[23] D. Gautam, M. Engenhorst, C. Schilling, G. Schierning, R. Schmechel, M. Winterer, Thermoelectric properties of pulsed current sintered nanocrystalline Al-doped ZnO by chemical vapour synthesis, J. Mater. Chem. (2015) 189–197, https://doi.org/10.1039/C4TA04355C.

[24] K.H. Kim, S.H. Shim, K.B. Shim, K. Niihara, J. Hojo, Microstructural and thermo-electric characteristics of zinc oxide-based thermoelectric materials fabricated using a spark plasma sintering process, J. Am. Ceram. Soc. (2005) 628–632, https://doi.org/10.1111/j.1551-2916.2005.00131.x.

[25] Y. Kinemuchi, H. Nakano, M. Mikami, K. Kobayashi, K. Watari, Y. Hotta, Enhanced boundary-scattering of electrons and phonons in nanograined zinc oxide, J. Appl. Phys. (2010) 53721, https://doi.org/10.1063/1.3475650.

[26] X. Liang, Thermoelectric transport properties of naturally nanostructured Ga–ZnO ceramics: effect of point defect and interfaces, J. Eur. Ceram. Soc. (2016) 1643–1650, https://doi.org/10.1016/j.jeurceramsoc.2016.02.017.

[27] M. Søndergaard, E.D. Bøjesen, K.A. Borup, S. Christensen, M. Christensen, B.B. Iversen, Sintering and annealing effects on ZnO microstructure and thermo-electric properties, Acta Mater. (2013) 3314–3323, https://doi.org/10.1016/j.actamat.2013.02.021.

[28] R.V.R. Virtudazo, Q. Guo, R. Wu, T. Takei, T. Mori, An alternative, faster and simpler method for the formation of hierarchically porous ZnO particles and their thermoelectric performance, RSC Adv. (2017) 31960–31968, https://doi.org/10.1039/c7ra05067d.

[29] K. Mahmood, M. Asghar, A. Ali, M. Ajaz-Un-Nabi, M.I. Arshad, N. Amin, et al., Enhancement of thermoelectric properties of MBE grown un-doped ZnO by thermal annealing, Advances In Energy Research (2015) 117–124, https://doi.org/10.12989/eri.2015.3.2.117.

[30] Y. Lan, A.J. Minnich, G. Chen, Z. Ren, Enhancement of thermoelectric figur-e-of-merit by a bulk nanostructuring approach, Adv. Funct. Mater. (2010) 357–376, https://doi.org/10.1002/adfm.200901512.

[31] A. Minnich, M. Dresselhaus, Z. Ren, G. Chen, Bulk nanostructured thermoelectric materials: current research and future prospects, Energy Environ. Sci. (2009) 466–479, https://doi.org/10.1039/B822664B.

[32] P. Radingoana, S. Guillemet-Fritsch, P. Olubambi, G. Chevallier, C. Estournès, Influence of processing parameters on the densification and the microstructure of pure zinc oxide ceramics prepared by spark plasma sintering, Ceram. Int. (2019) 10035–10043, https://doi.org/10.1016/j.ceramint.2019.02.048.

[33] T. Misawa, N. Shikatani, Y. Kawakami, T. Enjoji, Y. Ohtsu, H. Fujita, Observation of internal pulsed current flow through the ZnO specimen in the spark plasma sin-tering method, J. Mater. Sci. (2009) 1641–1651, https://doi.org/10.1007/s10853-008-2906-5.

[34] S. Yang, F. Chen, Q. Shen, L. Zhang, Microstructure and electrical property of aluminum doped zinc oxide ceramics by isolating current under spark plasma sin-tering, J. Eur. Ceram. Soc. (2016) 1953–1959, https://doi.org/10.1016/j.jeurceramsoc.2016.02.027.

[35] R. Chaim, G. Chevallier, A. Weibel, C. Estournès, Grain growth during spark plasma and flash sintering of ceramic nanoparticles: a review, J. Mater. Sci. (2018)

[36] R. Chaim, R. Marder, C. Estournés, Z. Shen, Densification and preservation of ceramic nanocrystalline character by spark plasma sintering, Advances in Applied Ceramics (2012) 280–285, https://doi.org/10.1179/1743676111Y.0000000074.

[37] R.M. German, Sintering Theory and Practice, (1996).

[38] M.N. Rahaman, Sintering of Ceramics, CRC Press, Nee York, 2008.

[39] M. Tokita, Mechanism of spark plasma sintering, Proceeding of NEDO International Symposium on Functionally Graded Materials: Japan, 1999, p. 22.

[40] R. Chaim, M. Levin, A. Shlayer, C. Estournès, Sintering and densification of nano-crystalline ceramic oxide powders: a review, Advances in Applied Ceramics (2008) 159–169, https://doi.org/10.1179/174367508X297812.

[41] T. Senda, R.C. Bradt, Grain growth in sintered ZnO and ZnO-Bi2O3 ceramics, J. Am. Ceram. Soc. (1990) 106–114, https://doi.org/10.1111/j.1151-2916.1990.tb05099.x.

[42] T. Gupta, R. Coble, Sintering of ZnO: I, Densification and grain growth, J. Am. Ceram. Soc. (1968) 521–525, https://doi.org/10.1111/j.1151-2916.1968.tb15679.x.

[43] V. Lee, G. Parravano, Sintering reactions of zinc oxide, J. Appl. Phys. (1959) 1735–1740, https://doi.org/10.1063/1.1735046.

[44] W. Luo, J. Pan, Effects of surface diffusion and heating rate on first-stage sintering that densifies by grain-boundary diffusion, J. Am. Ceram. Soc. (2015) 3483–3489, https://doi.org/10.1111/jace.13662.

[45] L. Han, N. Van Nong, W. Zhang, L.T. Hung, T. Holgate, K. Tashiro, et al., Effects of morphology on the thermoelectric properties of Al-doped ZnO, RSC Adv. (2014) 12353–12361, https://doi.org/10.1039/C3RA47617K.

[46] D.-B. Zhang, H.-Z. Li, B.-P. Zhang, H-d Liang, M. Xia, Hybrid-structured ZnO ther-moelectric materials with high carrier mobility and reduced thermal conductivity, RSC Adv. (2017) 10855–10864, https://doi.org/10.1039/C6RA28854E.

[47] A. Aimable, H. Goure Doubi, M. Stuer, Z. Zhao, P. Bowen, Synthesis and sintering of ZnO nanopowders, Technologies 28 (2017), https://doi.org/10.3390/technologies5020028.

[48] C. Lin, B. Wang, Z. Xu, H. Peng, Densification and electrical properties of zinc oxide varistors microwave-sintered under different oxygen partial pressures, J. Electron. Mater. (2012) 3119–3124, https://doi.org/10.1007/s11664-012-2191-6.

[49] Z. Chen, S. Yamamoto, M. Maekawa, A. Kawasuso, X. Yuan, T. Sekiguchi, Postgrowth annealing of defects in ZnO studied by positron annihilation, x-ray diffraction, Rutherford backscattering, cathodoluminescence, and Hall measure-ments, J. Appl. Phys. (2003) 4807–4812, https://doi.org/10.1063/1.1609050.

[50] D. Lisjak, I. Zajc, M. Drofenik, J. Jamnik, Investigation of the PTCR effect in ZnO–NiO two-phase ceramics, Solid State Ion. (1997) 125–135, https://doi.org/10.1016/S0167-2738(97)00197-5.

[51] T.K. Roy, D. Sanyal, D. Bhowmick, A. Chakrabarti, Temperature dependent re-sistivity study on zinc oxide and the role of defects, Mater. Sci. Semicond. Process. (2013) 332–336, https://doi.org/10.1016/j.mssp.2012.09.018.

[52] C.L. Cramer, J. Gonzalez-Julian, P.S. Colasuonno, T.B. Holland, Continuous func-tionally graded material to improve the thermoelectric properties of ZnO, J. Eur. Ceram. Soc. (2017) 4693–4700, https://doi.org/10.1016/j.jeurceramsoc.2017.07.019.

[53] A. Zakutayev, N.H. Perry, T.O. Mason, D.S. Ginley, S. Lany, Non-equilibrium origin of high electrical conductivity in gallium zinc oxide thin films, Appl. Phys. Lett. (2013) 232106, https://doi.org/10.1063/1.4841355.